

Supplementary information for

Excited States Engineering Enables Efficient Near-Infrared Lasing in Nanographenes

Giuseppe M. Paternò^{1§}, Qiang Chen^{2§†}, Rafael Muñoz-Mármol^{3§}, Michele Guizzardi⁴, Victor Bonal³, Ryota Kabe⁵, Alexander J. Barker, Pedro G. Boj⁶, Shreyam Chatterjee⁷, Yutaka Ie⁷, José M. Villalvilla³, José A. Quintana⁶, Francesco Scognella⁴, Klaus Müllen^{2,8}, María A. Díaz-García^{3*}, Akimitsu Narita^{2,9*} and Guglielmo Lanzani^{1,4*}

¹Center for Nano Science and Technology, Istituto Italiano di Tecnologia (IIT), Via Pascoli 10, 20133, Milano, Italy

²Max Planck Institute for Polymer Research, Ackermannweg 10, 55128, Mainz, Germany

³Departamento de Física Aplicada and Instituto Universitario de Materiales de Alicante, Universidad de Alicante, 03080 Alicante, Spain

⁴Physics Department, Politecnico di Milano, Piazza L. da Vinci 32, 20133 Milano, Italy

⁵Organic Optoelectronics Unit, Okinawa Institute of Science and Technology Graduate University, 1919-1 Tancha, Onna-son, Okinawa 904-0495, Japan

⁶Departamento de Óptica, Farmacología y Anatomía and Instituto Universitario de Materiales de Alicante, Universidad de Alicante, 03080 Alicante, Spain

⁷The Institute of Scientific and Industrial Research (SANKEN), Osaka University, 8-1 Mihogaoka, Ibaraki, Osaka 567-0047, Japan

⁸Institute of Physical Chemistry, Johannes Gutenberg University Mainz, Duesbergweg 10-14, 55128 Mainz, Germany

⁹Organic and Carbon Nanomaterials Unit, Okinawa Institute of Science and Technology Graduate University, 1919-1 Tancha, Onna-son, Okinawa 904-0495, Japan

[§] These authors contributed equally to this work

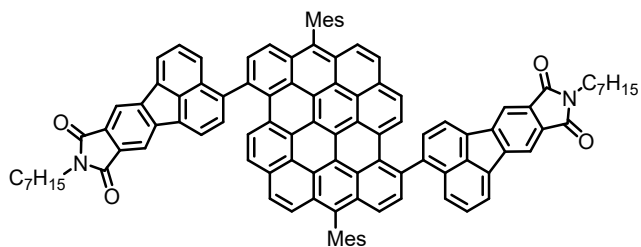
[†]Current affiliation Department of Chemistry, University of Oxford, Oxford OX1 3TA, U.K.

*Authors to whom correspondence should be addressed: maria.diaz@ua.es, akimitsu.narita@oist.jp and guglielmo.lanzani@iit.it

Materials and Method

Synthesis. All reactions working with air- or moisture- sensitive compounds were carried out under argon atmosphere using standard Schlenk line techniques. Thin layer chromatography (TLC) was done on silica gel coated aluminum sheets with F254 indicator and column chromatography separation was performed with silica gel (particle size 0.063–0.200 mm). Nuclear magnetic resonance (NMR) spectra were recorded on a Bruker Avance 500 MHz spectrometer. Chemical shifts (δ) were reported in ppm relative to the residual of solvents ($C_2D_2Cl_4$, 1H : 6.00 ppm, ^{13}C : 73.78 ppm). Abbreviations: s = singlet, d = doublet, m = multiplet. Coupling constants (J) were presented in Hertz. High-resolution mass spectrometry (HRMS) was performed on a SYNAPT G2-Si high resolution time-of-flight mass spectrometer (Waters Corp., Manchester, UK) by matrix-assisted laser desorption/ionization (MALDI), calibrated against poly(ethylene glycol). All commercially available chemicals were purchased from TCI, Aldrich, Acros, Merck, and other commercial suppliers and used without further purification. 3,11-Dibromo-6,14-dimesityldibenzo[*hi,st*]ovalene and fluoranthenediimide (FAI)-pinacol borate ester were prepared following the literature reported procedures.^{1,2}

Synthesis of DBOV-FAI:



A degassed suspension of 3,11-dibromo-6,14-dimesityldibenzo[*hi,st*]ovalene¹ (8.0 mg, 10 µmol), fluoranthenediimide (FAI)-pinacol borate ester² (25 mg, 50 µmol), Pd(PPh₃)₄ (2.3 mg, 2.0 µmol) and K₂CO₃ (14 mg, 0.10 mmol) in a mixture of toluene/ethanol/water = 10 mL/2.5 mL/2.5 mL was heated at 90 °C for 24 h. After cooling down to room temperature, water (20 mL) was added, and the mixture was extracted with ethyl acetate (20 mL) for three times. The separated organic phases were combined, washed with brine, dried over MgSO₄ and evaporated. The blue residue was purified by silica gel column chromatography (eluent: *n*-hexane:tetrahydrofuran = 5:1) and then recrystallized from dichloromethane and methanol to give the title compound (7.2 mg, 50% yield) as blue solid. ¹H NMR (500 MHz, C₂D₂Cl₄:CS₂ = 2:1) δ 8.60 – 8.67 (m, 2H), 8.46 (s, 2H), 8.43 – 8.37 (m, 4H), 8.20 – 8.15 (m, 3H), 8.13 (d, *J* = 7.6 Hz, 3H), 8.06 (d, *J* = 8.4 Hz, 2H), 8.00 (d, *J* = 8.2 Hz, 1H), 7.98 – 7.93 (m, 3H), 7.88 – 7.81 (m, 4H), 7.57 – 7.48 (m, 2H), 7.27 (s, 4H), 4.49 – 4.39 (m, 2H), 2.60 (s, 6H), 2.24 – 2.10 (m, 2H), 2.10 – 1.99 (m, 12H), 1.88 – 1.82 (m, 2H), 1.60 (d, *J* = 6.9 Hz, 6H), 1.45 – 1.35 (m, 12H), 0.97 (t, *J* = 6.6 Hz, 6H); ¹³C NMR (126 MHz, C₂D₂Cl₄:CS₂ = 2:1) δ 168.37, 152.53, 147.25, 146.25, 144.68, 144.28, 137.73, 135.50, 134.59, 134.16, 133.90, 132.86, 131.58, 130.90, 130.39, 129.12, 128.95, 128.52, 127.93, 126.96, 126.24, 125.53, 125.03, 124.63, 124.22, 123.96, 123.54, 123.07, 122.82, 116.16, 47.66, 34.09, 31.85, 30.07, 26.87, 23.04, 21.66, 20.90, 20.48, 18.99, 14.42; HRMS (MALDI-TOF, positive) *m/z*: Calcd for C₁₀₆H₇₈N₂O₄: 1442.5962; Found: 1442.6043 [M]⁺.

Optical characterisation. Absorption spectra were recorded on a Perkin-Elmer Lambda 900 spectrometer at room temperature using a 10 mm quartz cell. Emission spectra were recorded on a J&MTIDAS spectrofluorometer. Absolute photoluminescence quantum yields (PLQY) were measured using an integrating sphere with a photoluminescence measurement unit (Quantaurus-QY, C11347-01, Hamamatsu Photonics). Samples were dissolved in degassed toluene and photoexcited at 600 nm. Photoluminescence lifetime was measured using a streak camera system (C14832-110, Hamamatsu Photonics). A degassed toluene solution of sample was photoexcited by 343-nm femtosecond (pulse width 190 fs, 1 kHz) laser (Pharos and HERO, Light Conversion).

DFT. We have sketched the molecule geometries with the Avogadro package. We have optimized the ground state geometries and we have calculated the electronic transitions of the molecules with the package ORCA 4.2.1.³ We have used the B3LYP functional⁴ in the framework of the density functional

theory. We have employed the Ahlrichs split valence basis set⁵ and the all-electron nonrelativistic basis set SVPalls.^{6,7} Moreover, the calculation utilizes the Libint library⁸ and the Libxc library.^{9,10}

Transient absorption spectroscopy. For the non-degenerate pump and probe measurements, the molecule was dissolved in toluene with a concentration of 0.02 mg mL⁻¹. We employed an amplified Ti:sapphire laser with 2 mJ output energy, 1 kHz repetition rate and a central energy of 1.59 eV (800 nm). We used a pump wavelength of 390 nm and 620 nm, with the former obtained by frequency doubling the fundamental line with a Barium Borate crystal (BBO), and the latter, which is resonant with the main $\pi \rightarrow \pi^*$ transition, generated by using a visible optical parameter amplifier (OPA). Pump pulses were focused on a 200 μm spot (diameter), keeping pump fluences at $\sim 50 \mu\text{J cm}^{-2}$. As a probe pulse, we used a broadband white light super-continuum generated in sapphire plate in the spectral region from 450 nm to 750 nm.

For long-delay transient absorption, the pump light is obtained from a Q-switched Nd:YVO₄ laser (fundamental wavelength 1064 nm). This laser is electronically triggered and synchronized to the femtosecond laser (which continues to provide the probe light pulses) via an electronic delay. The Q-switched pulses have a width of ≈ 700 ps FWHM, and the system has a combined time resolution and jitter of ≈ 200 ps. We pumped at 355 nm.

Thin-films and DFB lasers preparation. Thin films of polystyrene (PS) doped with DBOV-FAI or DBOV-Mes (1wt%) were fabricated by spin coating a toluene solution of the compounds over quartz substrates. The film thickness (h) was measured by an optical method from the interference pattern present in the transparent region of the absorption spectrum.¹¹ The distributed feedback (DFB) resonators were fabricated following the procedure previously reported^{12–14} constituted by several steps: (1) deposition of the photoresist layer by spin coating a hot water solution (40 °C) of the dichromated gelatin (DCG; 2.2wt%) over the active film; (2) 1D grating recording by holographic lithography (HL) with the light from an Ar laser (I-308C, Coherent, Santa Clara, USA) emitting at 364 nm and using a mirror forming a 90° angle with the sample holder to generate the interferometric pattern to register; (3) the DCG layer was desensitized in a cool water bath (15 °C) and transformed into a relief grating by dry etching inn an oxygen plasma using a surface treatment machine (Zepto, Diener Electronic, Germany). The final grating presents a depth of 90 nm.

ASE and lasing characterization. As excitation source, we used a built-in optical parametric oscillator (LT 2214, LOTIS TII, Belarus) pumped with a 10 Hz repetition rate pulsed Nd:YAG (LS-2137U, LOTIS TII, Belarus) operating at 355 nm. The temporal width (τ_p) at each pump wavelength (λ_{pump}) is listed in **Table S6**. For the ASE characterization the pump beam was (1) expanded and collimated with an inverted Galileo telescope, (2) cleaned by selecting the central part with a diaphragm and (3) projected onto the sample forming a stripe of $3.5 \times 0.5 \text{ mm}^2$ by using a cylindrical lens and a slit. The pump intensity was controlled by means of neutral density filters and the sample emission was collected

from the edge of the film with an optical fibre coupled to a spectrophotometer (USB 2000 + UV-VIS, Ocean Optics, Florida, USA) with a spectral resolution of 1.3 nm.

For DFB characterization, the pump beam impinges the sample forming a ~30° angle with the normal to the device surface after being focalized onto the sample by using a spherical lens, then, forming an ellipse of minor axis 1.1 mm. For a DFB operating in the second-order of diffraction the emission is perpendicular to the device surface and it was collected with an optical fibre coupled to a spectrometer (USB 2000 + UV-VIS, Ocean Optics, Florida, USA) with spectral resolution of 1.3 nm. The beam divergence of the DFB devices was determined from measurements of the far-field pattern with a digital CMOS camera (ORCA-spark C11440-36U, HAMAMATSU, Japan) in a direction perpendicular to the resonator grating lines.

Losses and gain calculation. A recently developed method^{15,16} was used to calculate gain and losses from the PL and ASE spectra. This method relies on an analytical model capable of describing the evolution of the ASE intensity with the excitation and constitutes a generalization of the model used for variable stripe length method. The method requires that special attention is paid to the collection of the PL and ASE spectra, *i.e.* the PL spectrum should be collected under back scattering configuration and might be corrected from reabsorption effects, and the ASE spectra should correspond to a single ASE variable pump intensity experiment and ideally at least one spectrum should appertain to an excitation intensity well-below threshold (with no evidences of spectral collapse). All these spectra are fitted with the model in a multi-step process: (1) the model fits the ASE spectra taken well-below the ASE threshold using the PL spectra as a constraint to extract α ; (2) the remaining ASE spectra are fitted retrieving g_{net} at each pump fluence with spectral resolution. The fit was performed by using a GUI provided by the developer of the method.

Supplementary Data

^1H and ^{13}C NMR

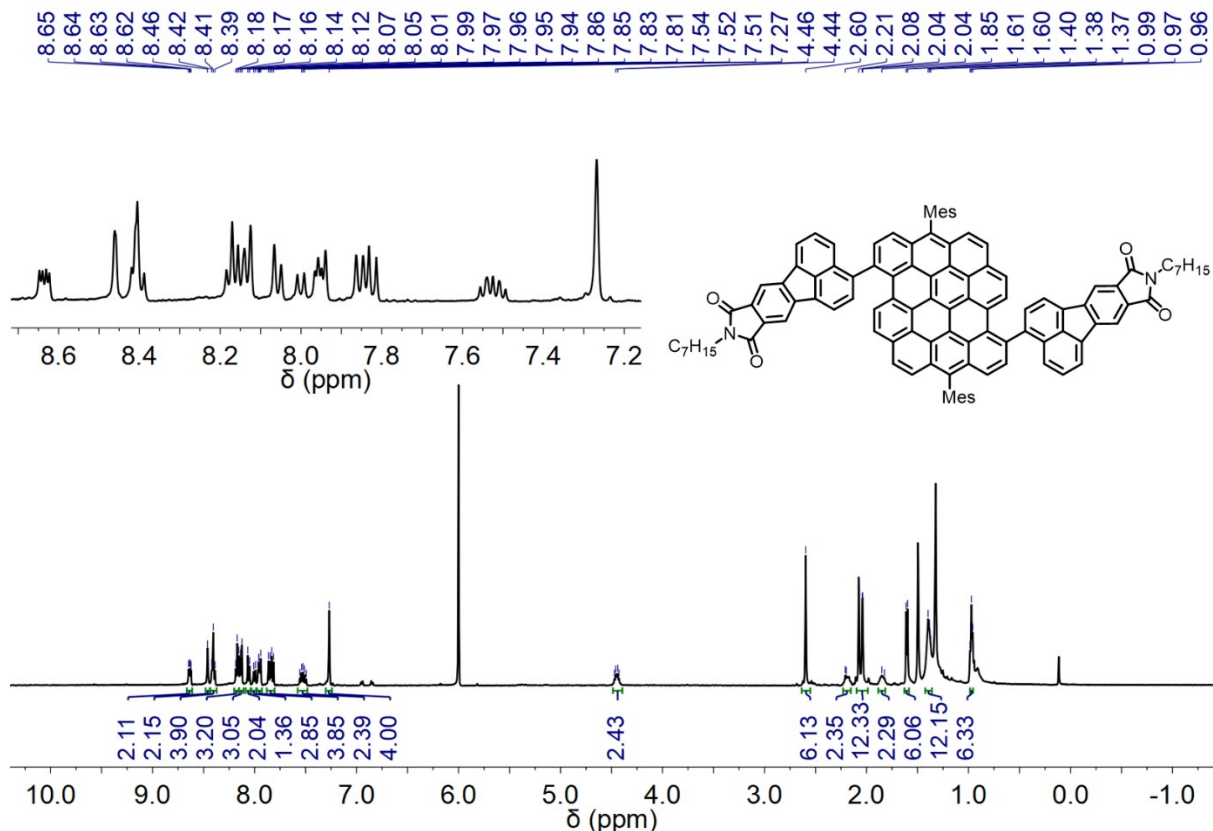


Figure S1. ^1H NMR spectrum of DBOV-FAI (500 MHz, $\text{C}_2\text{D}_2\text{Cl}_4:\text{CS}_2 = 2:1$, 303 K).

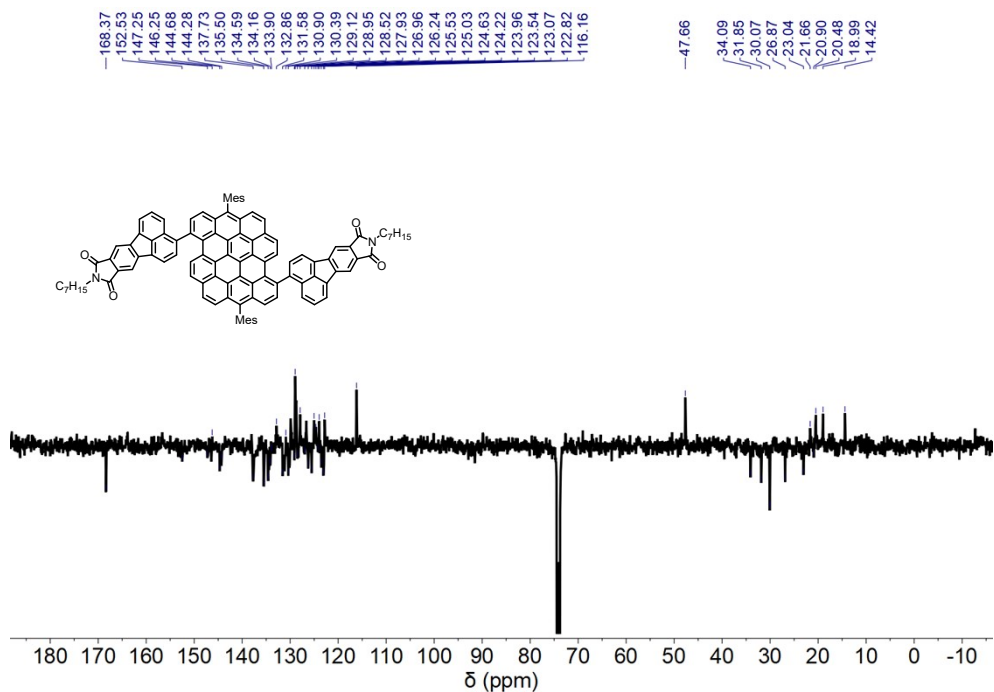


Figure S2. ^{13}C NMR (APT) spectrum of DBOV-FAI (126 MHz, $\text{C}_2\text{D}_2\text{Cl}_4:\text{CS}_2 = 2:1$, 303 K).

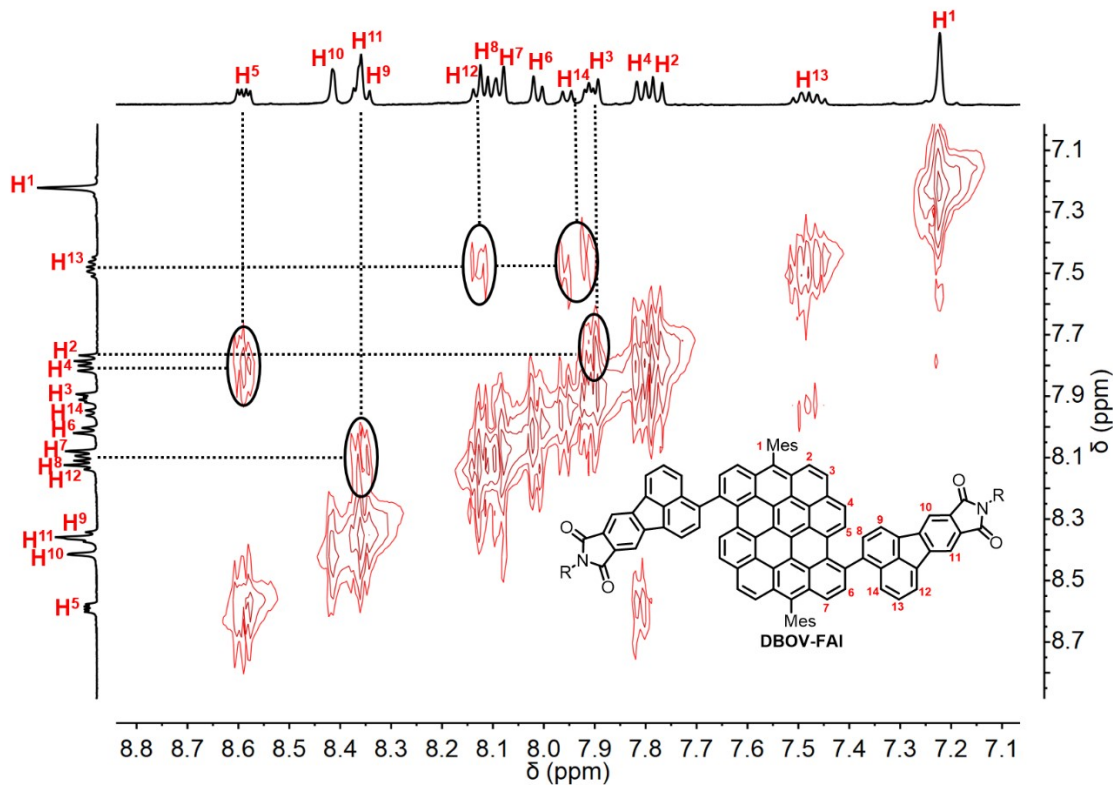


Figure S3. ^1H , ^1H -COSY spectrum of DBOV-FAI (500 MHz, $\text{C}_2\text{D}_2\text{Cl}_4:\text{CS}_2 = 2:1$, 303 K).

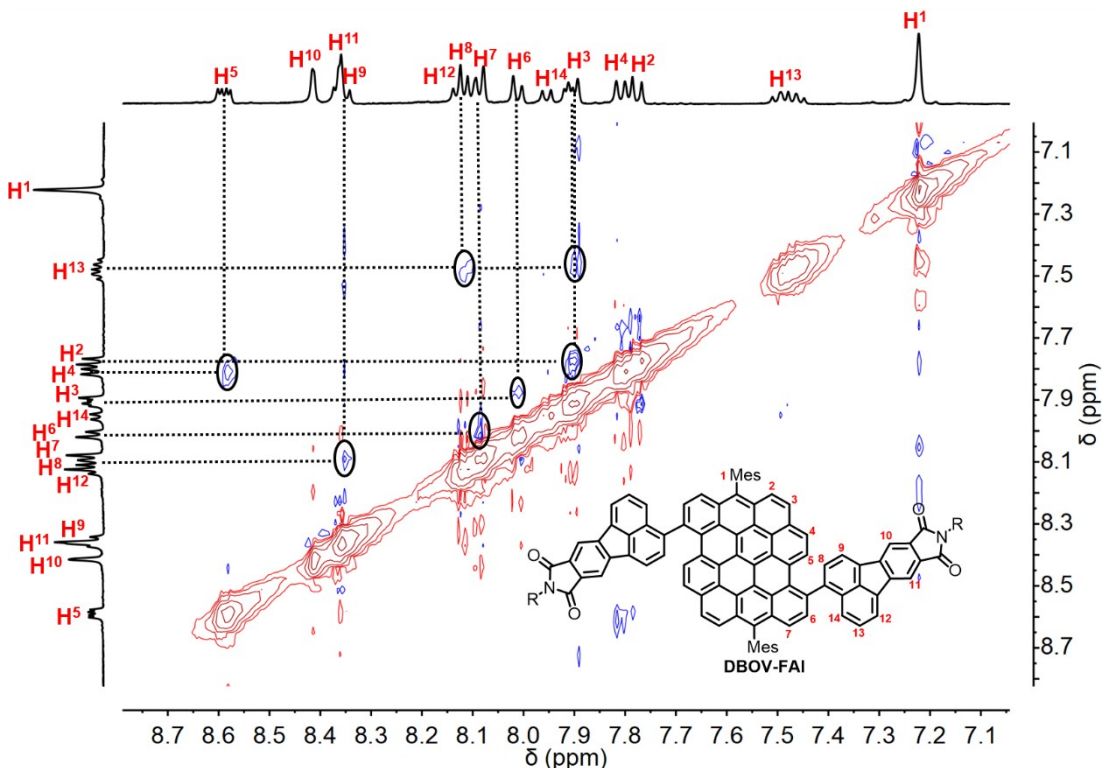


Figure S4. NOESY spectrum of DBOV-FAI (500 MHz, $\text{C}_2\text{D}_2\text{Cl}_4:\text{CS}_2 = 2:1$, 303 K).

Time-resolved photoluminescence

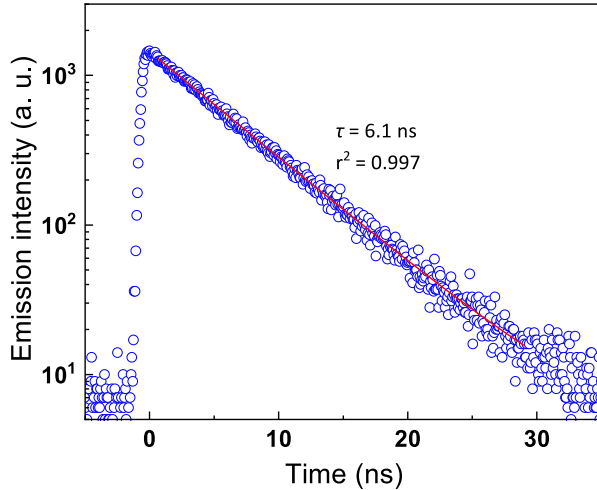


Figure S5. Emission decay profile of DBOV-FAI dissolved in degassed toluene. Sample was excited at 343 nm and emission intensity was integrated from 650 nm to 800 nm.

DFT calculations

For DBOV-FAI (blue dotted line), we computed two main transitions, namely: **transition 1** ($E=0.064454$ au, 1.754 eV) which involves the HOMO \rightarrow LUMO (weight 70%) and HOMO \rightarrow LUMO+2 (weight 30%); **transition 2** ($E= 0.066615$ au, 1.813 eV) that involves the HOMO \rightarrow LUMO+1 (see the main text for the frontier orbital profiles and energies).

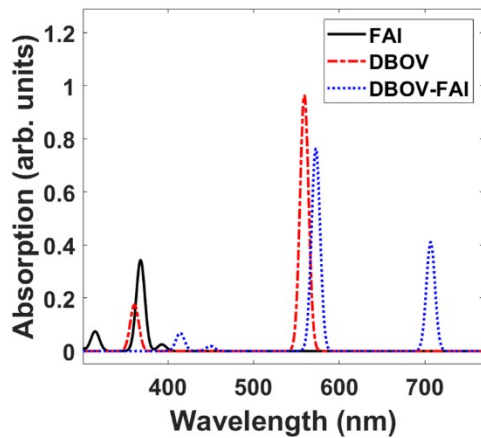


Figure S6. (a) Absorption spectra of FAI, DBOV-Mes and DBOV-FAI calculated by means of DFT method. The discrepancies between the simulated and experimental data, we think this is due to a number of effects, namely: i. the interaction with the molecule and its environment (i.e. solvatochromism); ii. the line broadening that has been arbitrarily assigned in the DFT calculation (5 nm) and that is very different to the experimental one; iii. vibrational relaxations that were not taken into account in the calculations. This is an important aspect, especially for such a complex molecule. See for instance the calculated transitions at 590 nm and 700 nm that are essentially merged in the experimental spectrum.

Table S1. Transition electric dipole moments for DBOV Mes.

State	Energy (cm ⁻¹)	Wavelength (nm)	fosc	T2 (au**2)	TX (au)	TY (au)	TZ (au)
1	17877.4	559.4	0.9638	17.74833	-1.03332	4.0841	0.02719
2	21835.8	458	1.33E-07	0	0.00047	-0.00133	0
3	22892	436.8	0.001466	0.02108	0.08665	-0.11591	0.01161
4	23246.3	430.2	6E-09	0	-0.00025	-0.00005	0.00015
5	25558.9	391.3	3.3E-08	0	0.00029	0.00058	0.00005
6	25868.5	386.6	1.9E-08	0	-0.0003	0.00033	-0.0002
7	26458.3	378	3.07E-05	0.00038	0.01403	-0.01285	0.00442
8	26471.4	377.8	0.000141	0.00175	0.03313	-0.02439	0.00762
9	27692.3	361.1	0.175087	2.08146	1.31195	0.50261	0.32805
10	27787.1	359.9	0.004933	0.05844	0.21692	0.08673	0.06214
11	27802.8	359.7	0.011582	0.13714	0.32898	0.13962	0.09704
12	28885.6	346.2	0.123776	1.41069	-1.1292	-0.24428	-0.27555
13	29022.6	344.6	5.19E-06	0.00006	-0.00734	-0.00177	-0.00134
14	30045.7	332.8	0.009964	0.10918	0.31333	0.07038	0.07777
15	30272.4	330.3	3.5E-08	0	0.0005	-0.00005	-0.00035
16	31192.2	320.6	0.051382	0.54231	-0.61606	-0.36756	-0.16636

Table S2. Transition electric dipole moments for DBOV FAI.

State	Energy (cm ⁻¹)	Wavelength (nm)	fosc	T2 (au**2)	TX (au)	TY (au)	TZ (au)
1	14146.1	706.9	0.410834	9.56102	1.50894	2.62186	0.64029
2	14620.3	684	1.54E-06	0.00003	-0.00261	-0.0048	-0.0022
3	17458.3	572.8	0.762804	14.38424	0.16841	-3.75596	-0.49866
4	21290.4	469.7	1.7E-08	0	0.00004	0.00049	0.00016
5	22229.6	449.9	0.018827	0.27881	-0.52091	-0.06255	-0.05965
6	22615	442.2	6.5E-08	0	-0.00055	-0.00015	-0.00079
7	23087.3	433.1	4.77E-07	0.00001	0.00198	0.00009	0.0017
8	24124.3	414.5	0.06781	0.92538	-0.6953	-0.62788	-0.2184
9	24127.1	414.5	0.000201	0.00274	0.03782	0.03442	0.01103
10	24516.9	407.9	0.001576	0.02116	-0.11592	-0.02226	-0.08502
11	24720.2	404.5	0.540402	7.19682	-2.59286	-0.39047	-0.56693
12	24759	403.9	6.07E-06	0.00008	0.00877	-0.00023	0.00194
13	24877.7	402	3.58E-06	0.00005	-0.00658	-0.0019	-0.00071
14	24973.9	400.4	0.271318	3.57659	1.80104	0.51606	0.25791
15	25145.1	397.7	0.14298	1.87196	1.12755	0.72298	0.27908
16	25313.5	395	2.9E-08	0	0.00042	0.00043	-0.00008

Table S3: Cartesian coordinates of the DFT-optimised FAI molecule.

		X	Y	Z
1	N	-4.41146	0.537462	-0.05624
2	C	-3.64548	1.712746	-0.05102
3	C	-3.64215	-0.63495	-0.05399
4	H	-5.42622	0.536003	-0.06165
5	C	-2.22251	-0.15986	-0.04645
6	C	-2.22509	1.242283	-0.04471
7	O	-4.07892	2.840123	-0.0518
8	O	-4.07111	-1.76403	-0.05765
9	C	-1.04527	1.983902	-0.03819
10	C	0.152576	1.261921	-0.0334
11	C	0.155536	-0.17604	-0.03511
12	C	-1.04161	-0.8996	-0.04173
13	H	-1.07086	3.077504	-0.03693
14	H	-1.06602	-1.99319	-0.0432
15	C	1.554225	1.715653	-0.02623

16	C	1.558923	-0.62668	-0.02891
17	C	2.359665	0.545868	-0.02371
18	C	2.184011	2.947596	-0.02197
19	C	3.603951	2.981566	-0.01565
20	C	4.413086	1.838824	-0.01274
21	C	3.767168	0.550427	-0.01682
22	C	4.385728	-0.73814	-0.01504
23	C	3.610832	-1.89094	-0.02022
24	C	2.188648	-1.8587	-0.02728
25	H	1.61948	3.884657	-0.02368
26	H	4.095277	3.959032	-0.01285
27	H	5.475137	-0.81203	-0.00955
28	H	1.623586	-2.79547	-0.03119
29	H	4.111617	-2.86431	-0.01878
30	B	5.959389	2.045621	-0.00429
31	O	6.529624	3.293358	0.012581
32	O	6.89534	1.040715	-0.01277
33	C	7.947224	3.152812	-0.04786
34	C	8.196509	1.624706	0.060336
35	H	8.409166	3.721782	0.777077
36	H	8.312197	3.573004	-1.00233
37	H	8.665762	1.338376	1.018864
38	H	8.820982	1.231639	-0.76009

Table S4. Cartesian coordinates of the DFT-optimised DBOV-Mes molecule.

1	C	-0.81752	-0.05179	0.594851
2	C	-1.51719	1.206981	0.517645
3	C	-0.82743	2.433585	0.755065
4	C	-1.54059	3.680765	0.669522
5	C	-0.83334	4.891138	0.904433
6	C	-2.93507	3.692415	0.354047
7	C	-3.6072	2.484062	0.125038
8	C	-2.89857	1.228173	0.203288
9	C	-3.59371	-0.00037	-0.03799
10	C	-2.90218	-1.25134	0.036683
11	C	-3.60374	-2.46867	-0.20721
12	C	-2.89049	-3.74804	-0.12584
13	C	-1.49245	-3.75012	0.197964

14	C	-5.01508	2.456535	-0.19547
15	C	-0.77958	-4.9974	0.284693
16	C	-0.80272	-2.52348	0.43525
17	C	0.614632	-5.00906	0.601303
18	C	0.578564	-2.54467	0.750097
19	C	0.582364	-0.06513	0.915847
20	C	0.570858	2.431594	1.077828
21	C	0.512911	4.872338	1.216263
22	C	1.286904	-3.80064	0.829498
23	C	1.273805	-1.31615	0.991083
24	C	1.283902	1.152158	1.159754
25	C	1.20842	3.65621	1.304092
26	C	2.694678	-3.77314	1.150323
27	C	2.664693	-1.33982	1.310473
28	C	2.655981	1.083997	1.475365
29	C	-3.52776	-4.97257	-0.35335
30	C	3.347945	-2.60151	1.380951
31	C	3.329386	-0.12534	1.549417
32	C	-2.83255	-6.18883	-0.26429
33	C	-1.48686	-6.20776	0.049747
34	C	-4.97604	-2.40054	-0.52177
35	C	-5.64951	-1.1912	-0.59544
36	C	-4.98473	0.02329	-0.35679
37	C	-5.66816	1.284907	-0.42661
38	C	-1.50227	-1.26469	0.357566
39	C	1.350244	-6.31492	0.688486
40	C	1.467943	-6.9803	1.928871
41	C	1.92952	-6.88184	-0.47167
42	C	2.162152	-8.1987	1.987562
43	C	2.613888	-8.09932	-0.36703
44	C	2.743412	-8.77681	0.853781
45	C	0.864317	-6.39395	3.185821
46	C	3.490186	-10.0886	0.932581
47	C	1.816404	-6.18962	-1.81168
48	C	-4.13452	4.868784	2.770292
49	C	-5.82962	8.761089	0.022678
50	C	-3.18002	5.086453	-2.22615
51	C	-4.47731	6.888133	-1.02395
52	C	-5.0604	7.46314	0.112315
53	C	-4.93062	6.783086	1.329978

54	C	-3.78696	5.669027	-0.96906
55	C	-4.24843	5.562328	1.431007
56	C	-3.67144	4.99813	0.270272
57	H	-1.36906	5.840239	0.835579
58	H	-5.55187	3.405687	-0.25065
59	H	1.0454	5.810907	1.397933
60	H	2.26879	3.687029	1.556429
61	H	3.231437	-4.72229	1.206196
62	H	3.217117	1.998213	1.670845
63	H	-4.58765	-5.00338	-0.60764
64	H	4.41438	-2.60126	1.627184
65	H	4.394815	-0.14129	1.798942
66	H	-3.36515	-7.12719	-0.4467
67	H	-0.9511	-7.15672	0.120405
68	H	-5.5374	-3.31482	-0.71632
69	H	-6.71513	-1.1753	-0.84417
70	H	-6.73465	1.284568	-0.67261
71	H	2.248709	-8.71022	2.95235
72	H	3.060773	-8.53125	-1.26937
73	H	1.316856	-5.41688	3.433553
74	H	1.015115	-7.06476	4.048498
75	H	-0.22091	-6.2203	3.07378
76	H	3.48608	-10.4962	1.957775
77	H	4.545202	-9.9713	0.621626
78	H	3.041664	-10.8482	0.265649
79	H	2.343231	-6.75739	-2.5968
80	H	2.246167	-5.17259	-1.781
81	H	0.762069	-6.07678	-2.12173
82	H	-4.65878	5.436945	3.556848
83	H	-3.08005	4.752954	3.078731
84	H	-4.56707	3.852969	2.739209
85	H	-5.44752	9.403442	-0.7899
86	H	-5.77298	9.33137	0.966449
87	H	-6.90237	8.577674	-0.18324
88	H	-3.33442	5.756381	-3.08886
89	H	-3.62714	4.106902	-2.47371
90	H	-2.09384	4.918439	-2.11408
91	H	-4.55853	7.404368	-1.98697
92	H	-5.37272	7.215145	2.23438

Table S5. Cartesian coordinates of the DFT-optimised DBOV-FAI molecule.

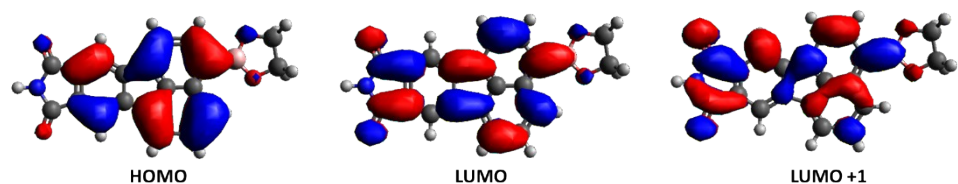
1	C	-0.80618	-0.20455	0.059687
2	C	-1.54633	1.030242	0.112587
3	C	-0.86832	2.282687	0.246656
4	C	-1.64529	3.492358	0.293704
5	C	-0.9664	4.726853	0.462783
6	C	-3.06941	3.454342	0.213069
7	C	-3.72592	2.220049	0.134808
8	C	-2.96415	0.995373	0.082145
9	C	-3.64776	-0.26175	0.022949
10	C	-2.91269	-1.48661	-0.07517
11	C	-3.6047	-2.73337	-0.16401
12	C	-2.85233	-3.9799	-0.37326
13	C	-1.41761	-3.93097	-0.23792
14	C	-5.16652	2.140054	0.133734
15	C	-0.64076	-5.14071	-0.28457
16	C	-0.73961	-2.67856	-0.10346
17	C	0.783315	-5.1028	-0.20282
18	C	0.678175	-2.64377	-0.07242
19	C	0.626782	-0.1617	0.084051
20	C	0.566515	2.331773	0.381098
21	C	0.390438	4.751875	0.688911
22	C	1.439867	-3.86855	-0.12434
23	C	1.36181	-1.38666	-0.01341
24	C	1.318832	1.085105	0.172302
25	C	1.17283	3.571236	0.705413
26	C	2.88047	-3.78866	-0.12231
27	C	2.787512	-1.35605	-0.06821
28	C	2.719328	1.069469	-0.00011
29	C	-3.45855	-5.21908	-0.69883
30	C	3.521451	-2.58872	-0.11303
31	C	3.435133	-0.11168	-0.10553
32	C	-2.67633	-6.39984	-0.68202
33	C	-1.31969	-6.37506	-0.45451
34	C	-5.00519	-2.71797	0.00859
35	C	-5.72101	-1.53694	0.114928
36	C	-5.07344	-0.29251	0.078208
37	C	-5.80743	0.940084	0.124166
38	C	-1.47973	-1.44375	-0.05077
39	C	1.567306	-6.38294	-0.23707

40	C	1.878366	-7.05191	0.968864
41	C	1.991965	-6.92512	-1.47204
42	C	2.607312	-8.24829	0.917044
43	C	2.719074	-8.12376	-1.4766
44	C	3.040957	-8.80177	-0.29416
45	C	1.436175	-6.49329	2.302961
46	C	3.856202	-10.0741	-0.32215
47	C	1.673899	-6.2296	-2.7766
48	C	-3.95605	4.581174	2.788058
49	C	-6.14292	8.42515	0.337024
50	C	-3.72582	4.844972	-2.29185
51	C	-4.89548	6.599608	-0.9042
52	C	-5.32747	7.152973	0.307616
53	C	-5.00383	6.474931	1.489601
54	C	-4.16642	5.403298	-0.9571
55	C	-4.27656	5.276445	1.483962
56	C	-3.85355	4.734359	0.248329
57	H	-1.54032	5.655717	0.471016
58	H	-5.73732	3.070184	0.162321
59	H	0.8824	5.703726	0.907526
60	H	3.451201	-4.71886	-0.14995
61	H	3.268784	2.004133	-0.06357
62	H	4.615094	-2.54217	-0.13816
63	H	4.523164	-0.07663	-0.2198
64	H	-3.16808	-7.35158	-0.90161
65	H	-0.74593	-7.30402	-0.46252
66	H	-5.55445	-3.65279	0.071518
67	H	-6.80901	-1.57204	0.229518
68	H	-6.90106	0.893476	0.14998
69	H	2.841839	-8.76341	1.854956
70	H	3.042389	-8.54002	-2.43681
71	H	1.867126	-5.49259	2.486368
72	H	1.748054	-7.15154	3.13102
73	H	0.338414	-6.378	2.353215
74	H	3.604746	-10.7349	0.525887
75	H	4.940305	-9.85643	-0.25649
76	H	3.694063	-10.6391	-1.25689
77	H	2.06778	-6.7989	-3.63488
78	H	2.113495	-5.21684	-2.81259
79	H	0.585125	-6.10804	-2.91861

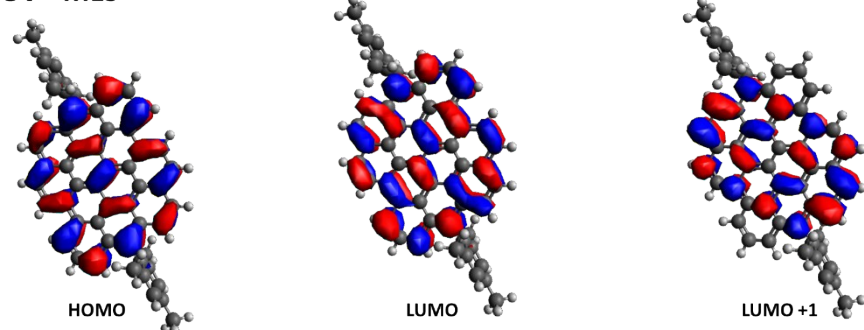
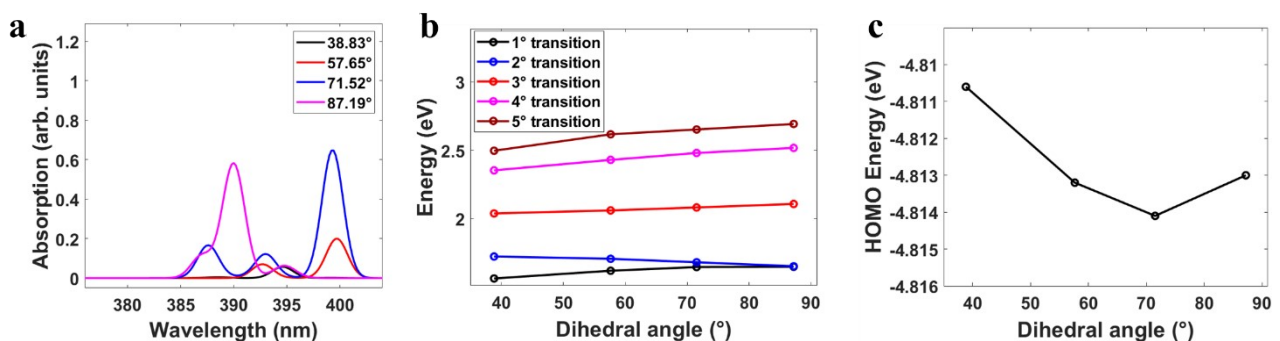
80	H	-4.35412	5.147219	3.646538
81	H	-2.86669	4.465895	2.931146
82	H	-4.38959	3.565791	2.822402
83	H	-5.89867	9.082444	-0.51577
84	H	-5.97329	8.994064	1.268067
85	H	-7.22746	8.206835	0.281324
86	H	-4.04034	5.50245	-3.11951
87	H	-4.15532	3.843468	-2.47419
88	H	-2.62793	4.731605	-2.34412
89	H	-5.13143	7.114715	-1.84174
90	H	-5.32594	6.891029	2.45029
91	N	-13.0419	-7.32459	-4.16604
92	C	-11.9994	-6.5798	-4.73728
93	C	-12.7263	-7.86111	-2.90866
94	C	-11.3248	-7.41029	-2.64238
95	C	-10.8905	-6.64443	-3.73406
96	O	-12.0303	-6.02267	-5.8083
97	O	-13.4567	-8.5355	-2.2229
98	C	-9.61827	-6.07869	-3.78304
99	C	-8.78286	-6.3099	-2.68438
100	C	-9.2279	-7.09754	-1.56539
101	C	-10.5105	-7.65477	-1.53821
102	H	-9.30131	-5.48574	-4.64524
103	H	-10.8713	-8.25475	-0.69834
104	C	-7.40624	-5.86856	-2.4069
105	C	-8.12879	-7.15289	-0.58503
106	C	-7.05751	-6.40297	-1.14026
107	C	-6.46381	-5.1015	-3.07127
108	C	-5.20138	-4.88606	-2.45977
109	C	-4.85053	-5.40706	-1.21127
110	C	-5.81507	-6.2103	-0.50773
111	C	-5.67327	-6.81097	0.77928
112	C	-6.71595	-7.54438	1.33178
113	C	-7.9566	-7.73155	0.660495
114	H	-6.66329	-4.6657	-4.05466
115	H	-4.4597	-4.28633	-2.99558
116	H	-4.74125	-6.68826	1.337256
117	H	-8.74805	-8.31704	1.13824
118	H	-6.58332	-7.99151	2.321342
119	O	9.751249	4.380675	5.80287

120	H	11.65812	5.820458	4.610046
121	N	10.76091	5.68029	4.157568
122	C	9.719026	4.936429	4.731172
123	C	10.44368	6.215234	2.899929
124	O	11.17322	6.888643	2.212314
125	C	8.60876	4.999912	3.72934
126	C	9.041817	5.764268	2.636089
127	C	7.336545	4.43445	3.780772
128	C	8.226021	6.007416	1.532661
129	C	6.499723	4.664345	2.682909
130	C	6.943436	5.450403	1.562278
131	C	5.122687	4.222824	2.4078
132	H	4.38169	3.02232	4.058139
133	C	4.181015	3.456789	3.074415
134	C	5.843073	5.504553	0.583256
135	C	2.917795	3.240637	2.464779
136	C	5.669429	6.081498	-0.66288
137	C	3.529184	4.562043	0.510121
138	C	2.565427	3.759916	1.215993
139	C	4.427924	5.893507	-1.33233
140	C	3.385862	5.160912	-0.77753
141	H	2.176755	2.641714	3.002376
142	C	4.772401	4.75555	1.140864
143	H	2.453217	5.037655	-1.33433
144	H	4.293972	6.339264	-2.32233
145	H	6.460359	6.666214	-1.14241
146	H	8.585853	6.606271	0.691552
147	H	7.020704	3.842733	4.644217
148	H	-13.9385	-7.46431	-4.61983

FAI



DBOV - MES

**Figure S7.** HOMO-LUMO distribution of FAI and DBOV - Mes based on DFT calculations.**Figure S8** Transitions upon excitation at 390 nm, alongside their oscillator strength. We can note that excitation to higher lying states populate more likely distorted states. (b) Transition energies and (c) HOMO energies as a function of the dihedral angle.

Ultrafast transient absorption

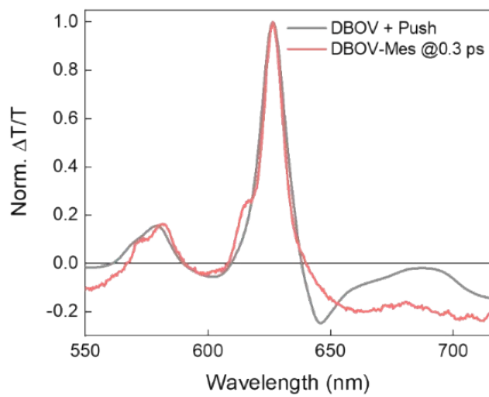


Figure S9. Comparison between the transient spectra of DBOV obtained via sequential pump-push excitation (610 nm excitation and 800 nm re-excitation, grey curve) and via direct excitation via a 390 nm excitation (red-curve). X-axis has been shifted by +10 nm for DBOV-Mes, to make the comparison clear.

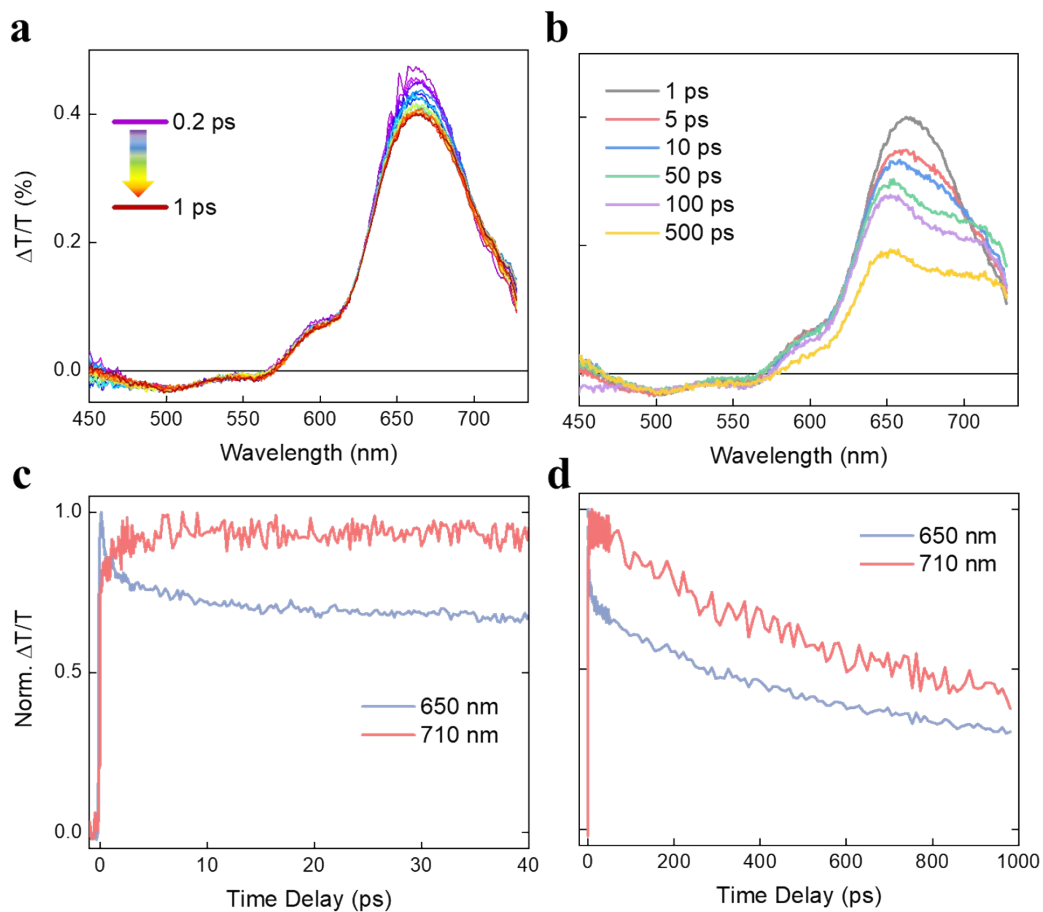


Figure S10. (a) Transient absorption spectra (excitation 640 nm) of DBOV-FAI at early pump-probe delays (0.2-1 ps.) and (b) from 1 ps to 500 ps. (c) Transient absorption dynamics at 650 nm (photobleaching signal, PB) and 710 nm (stimulated emission, SE) till 40 ps and (d) till 1 ns. Here, we can see that direct excitation to the LUMO level does not lead to the transfer mechanism, as the SE signal rises in ~ 2 ps.

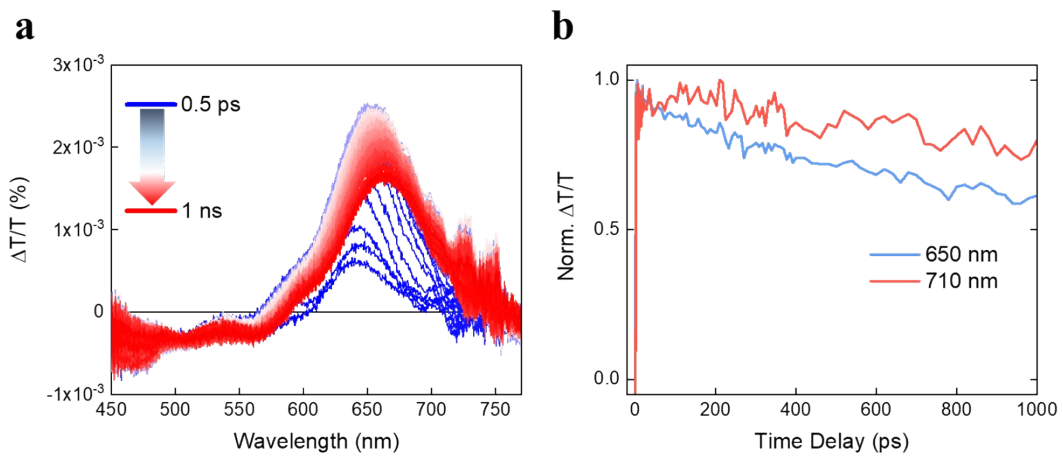


Figure S11. (a) Transient absorption spectra from 0.5 ps to 1 ns of DBOV-FAI dispersed in a polystyrene matrix (1% by weight) and (b) TA dynamics probe wavelengths of 650 nm (PB) and 710 nm (SE). The sample was excited at 390 nm.

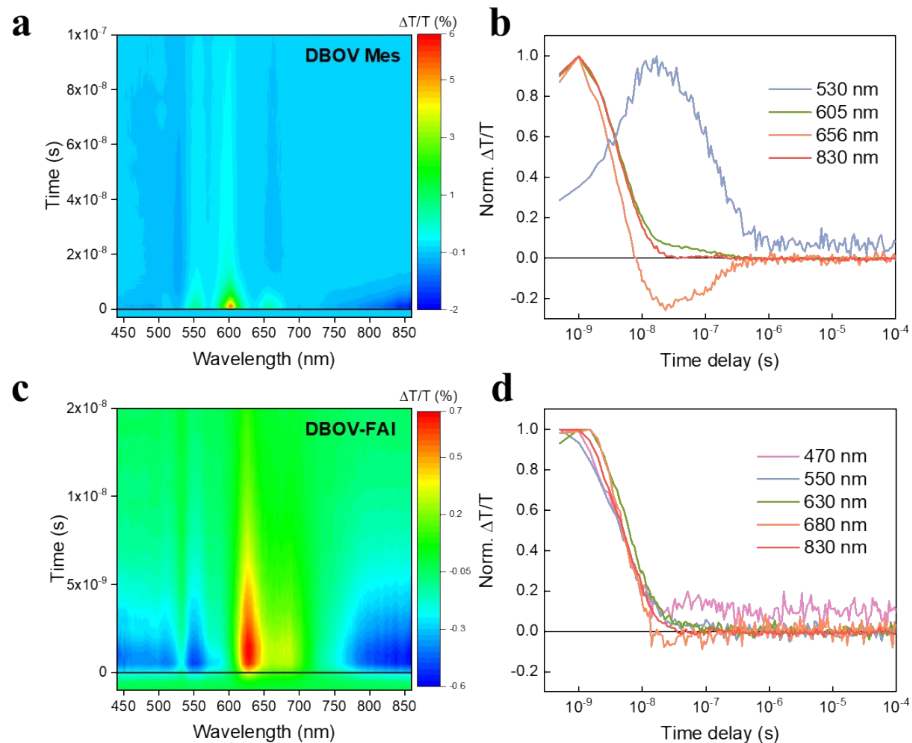
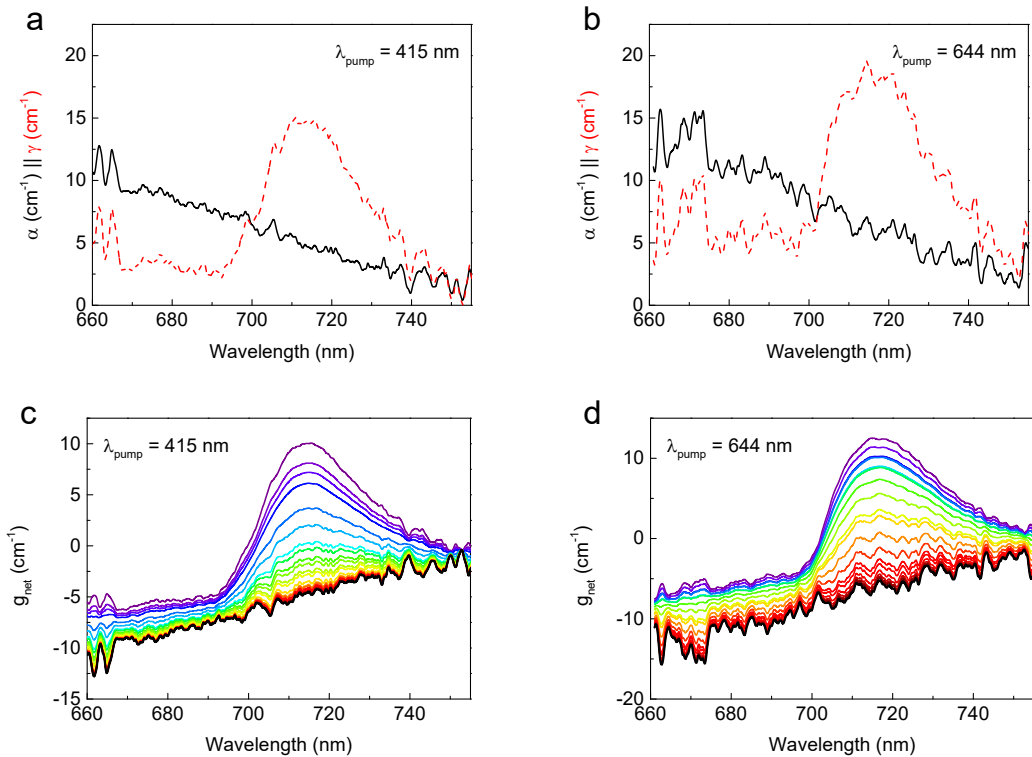
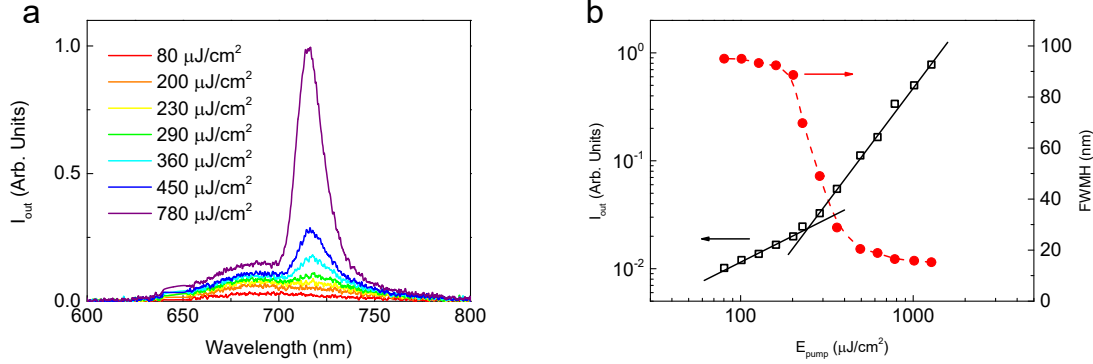
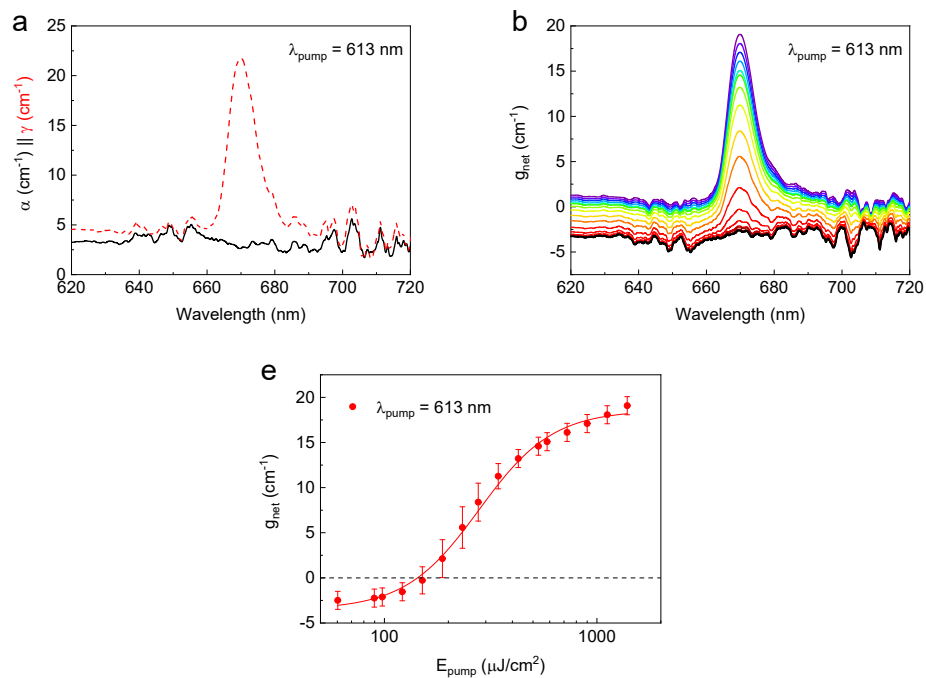
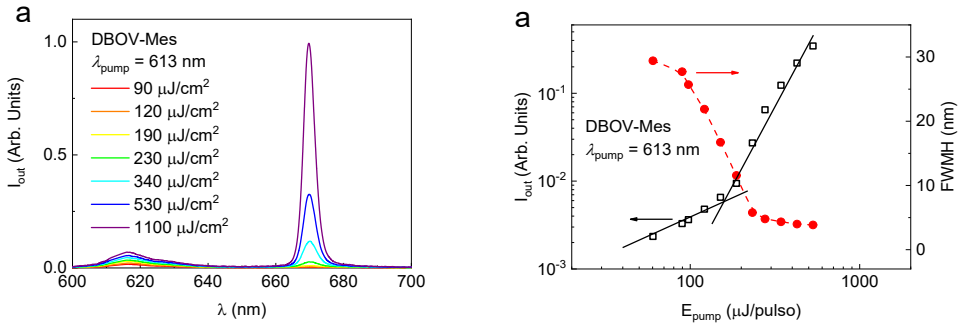


Figure S12. Long-dealy TA maps and dynamics (from 1 ns to 0.1 ms) for DBOV Mes (a,b) and DBOV FAI (c,d). The concentration of the two molecules is 0.02 mg/mL (toluene) and the excitation wavelength is 355 nm.

Amplified spontaneous emission





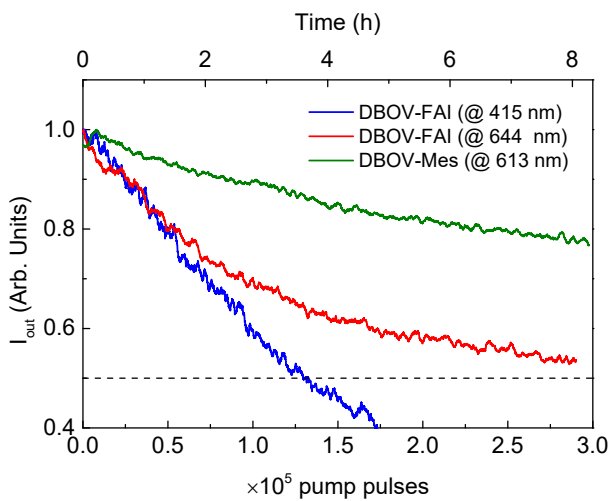
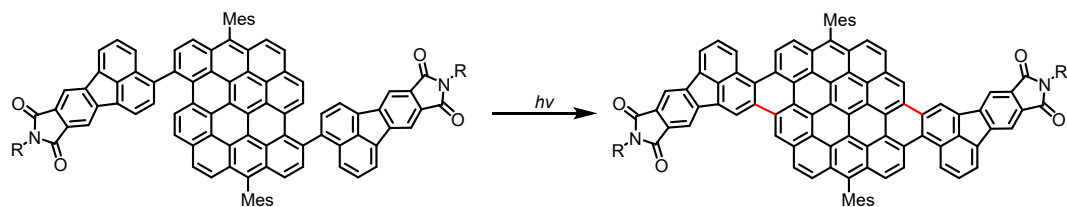


Figure S17. Amplified spontaneous emission (ASE) photostability for DBOV:polystyrene films (1 wt%). ASE output intensity normalized to its initial value versus time (top axis) and the number of pump pulses (bottom axis) under uninterrupted excitation with a fluence ~3-4 times the ASE threshold. DBOV-FAI doped films were analysed under 415 nm excitation (blue line) and 644 nm excitation (red line) and DBOV-Mes films under 613 nm excitation (green line). Black dashed line marks half the initial value. We note that DBOV FAI is in general less photostable than DBOV Mes. We reckon that DBOV-FAI might undergo ring-closing reaction between the DBOV core and the FAI units under high energy laser irradiation (see the scheme below). On the other hand, the single bonds between the DBOV core and FAI substituents could more easily be cleaved, generating reactive species and leading to degradation. These might make DBOV-FAI less stable than DBOV-Mes.



Scheme S1. Proposed side reaction that might occur for DBOV-FAI under high energy laser irradiation.

Table S6. Amplified spontaneous emission parameters.

	$\lambda_{\text{ABS}}^{\text{a}}$ (nm)	$\lambda_{\text{PL}}^{\text{b}}$ (nm)	h^{c} (nm)	$\lambda_{\text{pump}}^{\text{d}}$ (nm)	Abs. Coef. [$\lambda_{\text{pump}}^{\text{e}}$] ($\cdot 10^3$ cm $^{-1}$)	$\tau_p[\lambda_{\text{pump}}]^{\text{f}}$ (ns)	$\lambda_{\text{ASE}}^{\text{g}}$ (nm)	$\text{FWHM}_{\text{ASE}}^{\text{h}}$ (nm)	$E_{\text{th-ASE}}^{\text{i}}$ ($\mu\text{J}/\text{cm}^2$) ($\cdot 10^5$ pump pulses)	$\tau_{1/2}^{\text{j}}$
DBOV-FAI	644/590/ <u>388</u>	<u>684</u>	570	415	0.23	3.7	712	15	310	1.3
				644	0.28	4.6	714	15	270	3.5
DBOV-Mes	613/568/520	615/668	570	613	0.69	4.5	670	4	150	6.6

^aWavelengths of main absorption lines, the underlined value correspond with the larger peak. ^bWavelengths of main photoluminescence lines, the underlined value correspond with the larger peak. ^cFilm thickness (error ~2%). ^dPump wavelengths. ^eAbsorption coefficient at pump wavelength (error ~2%). ^fPump pulse width at pump wavelength. ^gASE wavelength (error ±0.7 nm). ^hASE linewidth (error ±1.3 nm) defined as the full width at half maximum well above the threshold. ⁱASE threshold (error ~20%). ^jThe photostability half-live parameter. The experiments have been realized pumping at 3-4 times $E_{\text{th-ASE}}$. Data for DBOV-Mes has been estimated from the extrapolation of the experimental data.

Lasing

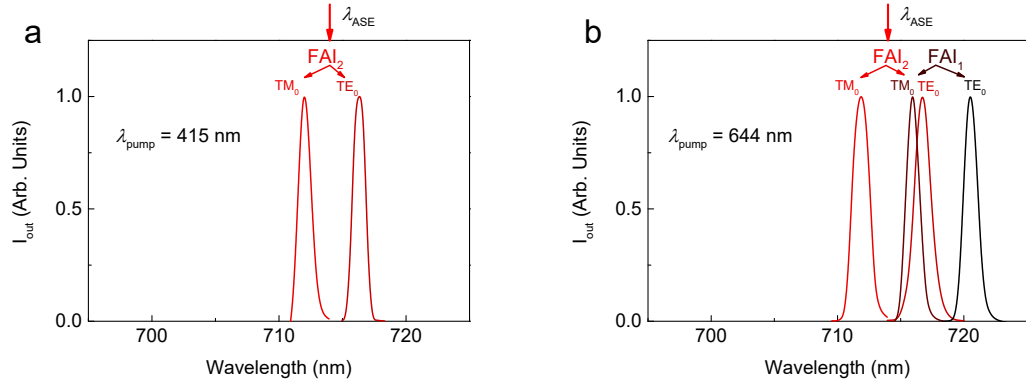


Figure S18. Laser modes observed in distributed feedback (DFB) lasers based on DBOV-FAI:polystyrene films (1 wt%) under (a) 415 nm and (b) 644 nm excitation. For each peak, its corresponding laser device and associated mode is indicated and the material ASE wavelength is marked by the arrow in top of the panel.

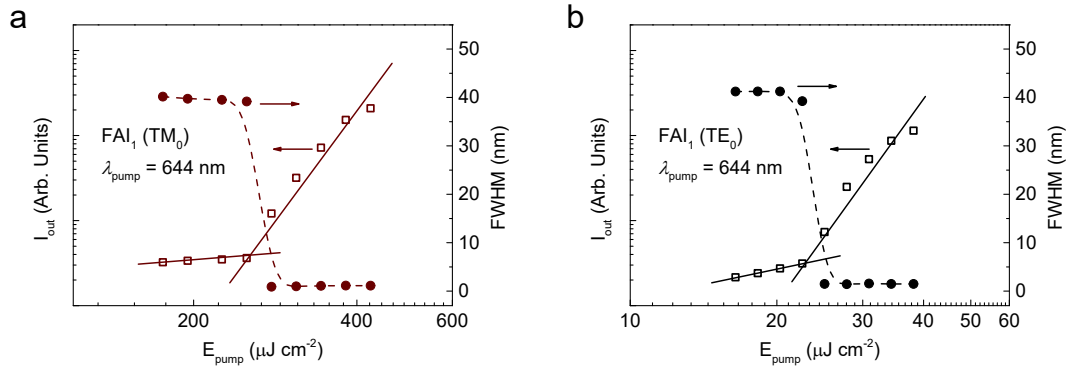


Figure S19. Threshold characterization of the first distributed feedback (DFB) laser (Device 1) based on DBOV-FAI:polystyrene films (1 wt%). Output intensity (I_{out} , left axis, open squares) and linewidth defined as the full width at half maximum (FWHM, right axis, full circles) as functions of pump energy density for TM₀ (a) and TE₀ (b) laser modes in the Device 1. The pump was at 644 nm. Lines are guides to the eye.

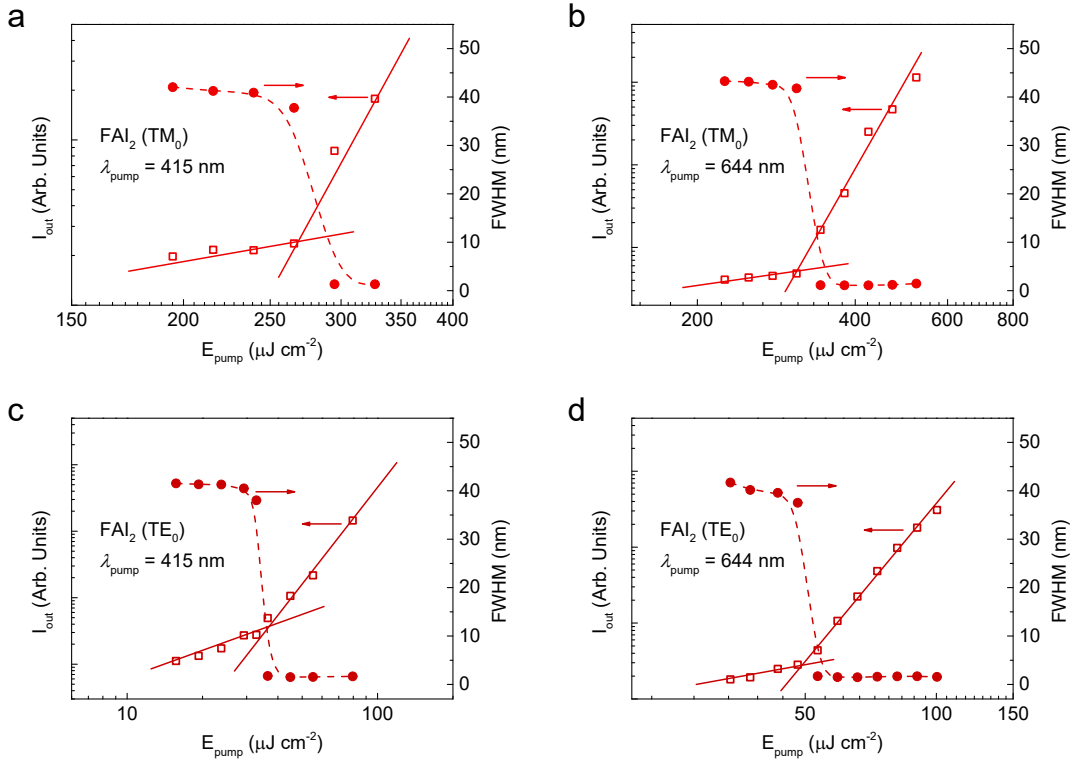


Figure S20. Threshold characterization of the second distributed feedback (DFB) laser (Device 2) based on DBOV-FAI:polystyrene films (1 wt%). Output intensity (I_{out} , left axis, open squares) and linewidth defined as the full width at half maximum (FWHM, right axis, full circles) as functions of pump energy density for TM_0 (a, b) and TE_0 (c, d) laser modes in the Device 2. The pump was at 415 nm (a, c) and 644 nm (b, d). Lines are guides to the eye.

Table S7. Parameters characterized for distributed feedback (DFB) lasers based on DBOV-FAI:polystyrene films (1 wt%).

Devices	h^{a} (nm)	Λ^{b} (nm)	$\lambda_{\text{pump}}^{\text{c}}$ (nm)	$\tau_{\text{p}}[\lambda_{\text{pump}}]^{\text{d}}$ (ns)	Mode ^e	$\lambda_{\text{DFB}}^{\text{f}}$ (nm)	$E_{\text{th-DFB}}^{\text{g}}$ ($\mu\text{J}/\text{cm}^2$)
Device 1	610	467.4	415	3.7	TM_0	716.3	250
			644	4.6	TE_0	720.3	60
	610	457.7	415	3.7	TM_0	716.0	280
			644	4.6	TE_0	720.7	25
Device 2	610	457.7	415	3.7	TM_0	711.9	300
			644	4.6	TE_0	716.3	50
	610	457.7	415	3.7	TM_0	711.9	340
			644	4.6	TE_0	716.6	50

^aFilm thickness (error ~2%). ^bGrating period (error ~0.5%). ^cPump wavelength. ^dPump pulse width at pump wavelength.

^eWaveguide mode associated to each laser peak. ^fDFB wavelength (error ±0.7 nm). ^gDFB threshold (error ~20%) expressed as energy density, $E_{\text{th-DFB}}$.

References

- 1 Q. Chen, D. Wang, M. Baumgarten, D. Schollmeyer, K. Müllen and A. Narita, *Chem. - An Asian J.*, 2019, **14**, 1703–1707.
- 2 S. Chatterjee, Y. Ie, T. Seo, T. Moriyama, G. J. A. H. Wetzelaer, P. W. M. Blom and Y. Aso, *NPG Asia Mater.*, 2018, **10**, 1016–1028.
- 3 F. Neese, *Wiley Interdiscip. Rev. Comput. Mol. Sci.*, 2012, **2**, 73–78.
- 4 C. Lee, W. Yang and R. G. Parr, *Phys. Rev. B*, 1988, **37**, 785–789.
- 5 A. Schäfer, H. Horn and R. Ahlrichs, *J. Chem. Phys.*, 1992, **97**, 2571–2577.
- 6 A. Schäfer, C. Huber and R. Ahlrichs, *J. Chem. Phys.*, 1994, **100**, 5829–5835.
- 7 K. Eichkorn, F. Weigend, O. Treutler and R. Ahlrichs, *Theor. Chem. Acc.*, 1997, **97**, 119–124.
- 8 F. Pavošević, F. Neese and E. F. Valeev, *J. Chem. Phys.*, 2014, **141**, 54106.
- 9 M. A. L. Marques, M. J. T. Oliveira and T. Burnus, *Comput. Phys. Commun.*, 2012, **183**, 2272–2281.
- 10 S. Lehtola, C. Steigemann, M. J. T. Oliveira and M. A. L. Marques, *SoftwareX*, 2018, **7**, 1–5.
- 11 V. Bonal, J. A. Quintana, R. Muñoz-Mármol, J. M. Villalvilla, P. G. Boj and M. A. Díaz-García, *Thin Solid Films*, 2019, **692**, 137580.
- 12 E. M. Calzado, J. M. Villalvilla, P. G. Boj, J. A. Quintana, P. A. Postigo and M. A. Díaz-García, *Appl. Opt.*, 2010, **49**, 463–470.
- 13 J. A. Quintana, J. M. Villalvilla, M. Morales-Vidal, P. G. Boj, X. Zhu, N. Ruangsrapichat, H. Tsuji, E. Nakamura and M. A. Díaz-García, *Adv. Opt. Mater.*, 2017, **5**, 1700238.
- 14 V. Bonal, J. A. Quintana, J. M. Villalvilla, P. G. Boj and M. A. Díaz-García, *Sci. Rep.*, 2019, **9**, 11159.
- 15 L. Cerdán, *Opt. Laser Technol.*, 2020, **121**, 105814.
- 16 L. Cerdán, M. Anni, M. L. De Giorgi, P. G. Boj and M. A. Díaz-García, *Opt. Laser Technol.*, 2021, **136**, 106766.